Journal of Magnetic Resonance Open 16–17 (2023) 100102

Contents lists available at ScienceDirect

Journal of Magnetic Resonance Open

journal homepage: www.sciencedirect.com/journal/journal-of-magnetic-resonance-open

An introduction to one- and two-dimensional lineshape analysis of chemically exchanging systems

Christopher A. Waudby [a,*], Ignacio Alfonso [b]

[a] School of Pharmacy, University College London, London, WC1N 1AX, United Kingdom
[b] Department of Biological Chemistry, Institute for Advance Chemistry of Catalonia (IQAC-CSIC), Jordi Girona 18-26, Barcelona, 08034, Spain

ARTICLE INFO

Keywords:
Lineshape analysis
Molecular interactions
Titrations
Ligand binding
Dynamic NMR

ABSTRACT

Molecules are dynamic entities, and understanding intra- and inter-molecular reactions and changes in conformation is one of the most fascinating, important and complex subjects in NMR. Conformational changes and chemical reactions result in observed spins exchanging between different magnetic environments, and the sensitivity of NMR spectra to such dynamic processes has been recognised since the earliest days of the field. Careful analysis of such spectra, acquired using one- or two-dimensional experiments, can provide insight into structural, thermodynamic, kinetic and mechanistic aspects of the underlying exchange process. The theoretical principles of these lineshape analysis methods will be introduced in this article, alongside a practical discussion of calculation methods, data acquisition and analysis software.

Introduction

Chemical exchange refers to a wide variety of processes by which spins interconvert between different magnetic environments. These processes may be intra- or inter-molecular, and covalent or non-covalent. Examples include bond rotation [1], fluxionality [2,3], sigmatropic shifts [4], ring flips [5], the exchange of labile protons with the solvent [6], protein folding and unfolding [7], intermediate formation [8], and ligand binding and host-guest recognition [9–11]. Exchange can occur over a wide range of timescales, from ps–ns (protein side chain rotations and loop motions), ns (rotational diffusion), μs–s or slower (protein folding, domain motions, and ligand binding), although the rate of these processes may vary substantially depending on the associated free energy barrier and temperature. NMR spectra and experiments can probe many aspects of the free energy landscapes that encode the behaviour of a molecule or molecules involved in such exchange processes. This includes structure (chemical shifts) and molecular weight (line widths), thermodynamics (populations, equilibrium constants), the kinetics of chemical exchange processes, and their mechanism (the number of states, and the pathways that connect them). This can often be done in a non-invasive way, observing processes at dynamic equilibrium without requiring physical perturbations or manipulation of a sample. Indeed, for processes occurring on rapid timescales such perturbations may not even be feasible experimentally. For this reason, NMR spectroscopy has become one of the most important methods available for studying exchange and dynamics, from small molecules to large biomolecular complexes.

In this article, we will introduce the characterisation of chemical exchange through one- and two-dimensional lineshape analysis. To this end, we first review basic aspects of chemical exchange, its impact on one- and two-dimensional NMR measurements, and then in turn survey the principles, calculation methods, and available software, for performing one- and two-dimensional lineshape analysis. In doing so, we hope that this article might encourage and facilitate the more widespread use of these powerful analytical methods.

A note on units

Before commencing, it is worth highlighting an aspect of units that can often cause confusion in discussions of chemical exchange: Hertz (Hz) versus inverse seconds (s^{-1}). While equivalent in terms of dimensional analysis, Hz refers specifically to linear frequency, being equivalent to one cycle per second. Such frequencies are commonly denoted by a lower-case nu (ν), and in NMR may be used to describe resonance frequencies and linewidths. In contrast, s^{-1} refers to angular frequency (i.e. radians per second), and is commonly denoted by a lower-case omega (ω). Linear and angular frequencies are related by a factor of 2π, $\omega = 2\pi\nu$. In contrast, relaxation rates (such as R_1 and R_2) and kinetic

* Corresponding author.
E-mail address: c.waudby@ucl.ac.uk (C.A. Waudby).

https://doi.org/10.1016/j.jmro.2023.100102

Available online 5 March 2023

rate constants are measured only in inverse seconds (s^{-1}): they are not frequencies and should not be reported in Hz.

Chemical exchange

When discussing chemical exchange, we refer to exchange between *states*, that is, minima in free energy landscapes. Importantly, state is a global property of a molecule: if a molecule exchanges between two states, A and B, then every spin in the molecule will have spectroscopic properties associated with both states (although it may turn out that these are very similar in regions of the molecule far from any conformational changes).

The rate of exchange between two states can be described with a first-order (or pseudo-first order) rate constant. For the irreversible unimolecular process $A \overset{k_{AB}}{\rightarrow} B$, we can write the rate of change of the concentration of A: $\frac{d[A]}{dt} = -k_{AB}[A]$. However, when studying chemical exchange by NMR we are generally concerned with reversible processes at equilibria:

$$A \underset{k_{BA}}{\overset{k_{AB}}{\rightleftharpoons}} B \tag{1}$$

The populations of A and B, p_A and p_B, are related to each other by the equilibrium constant K_{AB}. This is related to the free energy difference between the two states, as well as kinetically to the ratio of the rate constants:

$$K_{AB} = \frac{p_B}{p_A} = \frac{k_{AB}}{k_{BA}} = \exp\left(-\frac{\Delta G_{AB}}{RT}\right) \tag{2}$$

$$p_A = \frac{k_{BA}}{k_{AB} + k_{BA}} \tag{3}$$

$$p_B = \frac{k_{AB}}{k_{AB} + k_{BA}} \tag{4}$$

At equilibrium, the forwards and backwards flux across the equilibrium are equal ($p_A k_{AB} = p_B k_{BA}$). For highly skewed populations, this indicates that a slow reaction from a highly populated state is balanced by a rapid backwards reaction from a sparsely populated state.

Importantly, because molecules are indistinguishable, no experimental technique is able to observe the exchange of molecules between states in dynamic equilibrium: some form of perturbation is essential in order to probe the kinetics and mechanism of exchange. The great strength of NMR spectroscopy lies in the ability to apply a chemically inert magnetic perturbation to study chemical equilibria. By applying rf pulses to perturb the *magnetic* equilibrium, previously indistinguishable molecules can now be distinguished, and we can observe their flux through a reaction network.

Exchange of spin states

To analyse chemical exchange by NMR, chemical states must be mapped to spin states, i.e. to distinct magnetic environments experienced by the spins under observation (Fig. 2). Each spin state is associated with spectroscopic parameters such as chemical shifts, relaxation rates and coupling constants, the analysis of which can ultimately provide structural information in addition to thermodynamic and kinetic information. Multiple spins within a molecule, for example along the sequence of a polypeptide, can be treated independently and the results combined in a final analysis.

In general, this mapping is straightforward, e.g. for intramolecular exchange A⇌B (Eq. 1) the chemical states A and B correspond directly to spin states. For protein-observed ligand binding (Fig. 1A):

$$P + L \underset{k_{off}}{\overset{k_{on}}{\rightleftharpoons}} PL \tag{5}$$

we consider the two protein spin states P and PL, which exchange with pseudo-first order rates:

$$P \underset{k_{off}}{\overset{k_{on}[L]}{\rightleftharpoons}} PL \tag{6}$$

The free ligand concentration, [L], in this expression is calculated from the dissociation constant, $K_d = k_{off}/k_{on}$, and the total concentrations of protein, $[P]_0$, and ligand, $[L]_0$:

$$[L] = \frac{1}{2}\left([L]_0 - [P]_0 - K_d + \sqrt{([L]_0 - [P]_0 - K_d)^2 - 4[L]_0[P]_0}\right) \tag{7}$$

In other cases, such as dimerization, or the binding of a ligands to a dimer, a single chemical state may contain multiple spin states, which may or may not be magnetically equivalent depending on the symmetry of the dimer. Examples of this are illustrated in Fig. 1B and C.

Chemical exchange at dynamic equilibrium

An important property of chemical exchange at dynamic equilibrium is that kinetics are always linear, because the fluctuations in equilibrium concentrations as molecules exchange back and forth are negligible. The rate of change of the concentration of spin states can therefore always be expressed using pseudo-first order rate constants, in terms of gain and loss from and to other states [12].

An extensive literature is available reviewing and discussing the effects and analysis of chemical exchange on NMR spectra [13–17]. For the simplest example of two-state exchange (Eq. 1), we can write [15]:

$$\begin{aligned} \frac{dA}{dt} &= -k_{AB}A + k_{BA}B \\ \frac{dB}{dt} &= k_{AB}A - k_{BA}B \end{aligned} \tag{8}$$

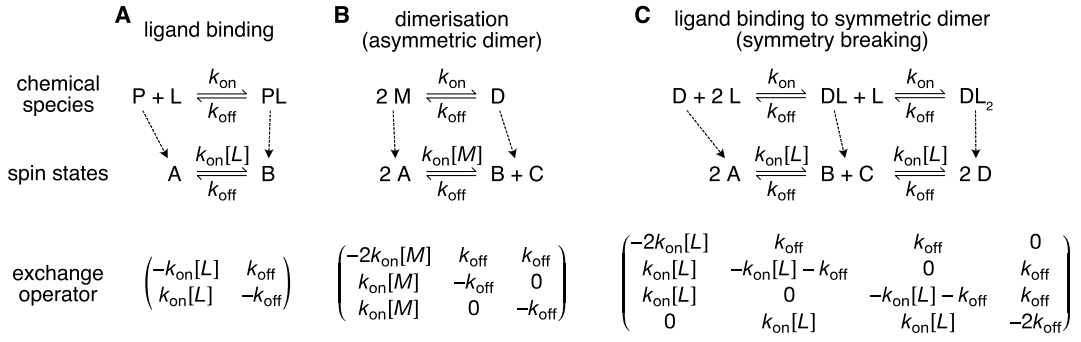

Fig. 1. Mapping chemical states and equilibria to spin states and pseudo-first order exchange rates. Three examples are shown: (A) simple two-state ligand binding; (B) association of monomers into an asymmetric dimer (spin states B and C); and (C) binding of two ligands to a symmetric dimer via an asymmetric, singly-bound intermediate (spin states B and C). The exchange operator, written in terms of the spin state populations A, B, …, is also shown for each example.

This enables kinetics to be expressed using a simple matrix formulation in terms of an exchange operator, K, acting on the space of spin states [15]:

$$\frac{d\vec{M}}{dt} = \frac{d}{dt}\begin{pmatrix} A \\ B \end{pmatrix} = \begin{pmatrix} -k_{AB} & k_{BA} \\ k_{AB} & -k_{BA} \end{pmatrix} \cdot \begin{pmatrix} A \\ B \end{pmatrix} = K \cdot \vec{M} \tag{9}$$

Eigenvalues of the exchange operator contain the chemical relaxation rates of the system, i.e. the rates of return to equilibrium following a perturbation (while eigenvectors contain the associated change in concentrations). An exchange operator will always contain one zero eigenvalue, representing the equilibrium state that does not change over time. The second eigenvalue for the operator above (Eq. 9), which for a two-state system is usually denoted simply as the exchange rate k_{ex}, is [15]:

$$k_{ex} = k_{AB} + k_{BA} \tag{10}$$

In the earlier example of a protein-ligand interaction (Eq. 6, Fig. 1A), this exchange rate is:

$$k_{ex} = k_{off} + k_{on}[L] \tag{11}$$

As the free ligand concentration [L] (Eq. 7) increases monotonically with the total ligand concentration, the exchange rate (Eq. 11) also always increases along the course of a titration (Fig. 2).

Knowledge of these exchange rates is critical to understanding chemical exchange in NMR, as they are the quantities against which differences in spectroscopic parameters are compared in order to define *fast, intermediate* and *slow* exchange regimes. For more complex exchange mechanisms, there may be more than one exchange rate (i.e. the exchange operator may have multiple distinct, non-zero eigenvalues). In such cases, exchange may be in different regimes with respect to each chemical relaxation process [18].

Chemical exchange in NMR

Chemical exchange can affect NMR experiments in a variety of ways, most obviously in the free induction decay and its associated spectrum. Here, chemical exchange can lead to distinct resonances appearing for each exchanging state, to a single resonance at a population-weighted average position, or to severe line broadening of exchanging resonances. It is worth noting that NMR is unique in this amongst spectroscopic methods, such as fluorescence or circular dichroism spectroscopy, which observe only the combined spectra of species populated at a given instant. This ultimately reflects the small energy differences and long lifetimes associated with nuclear spin states.

A central concept in understanding the effect of chemical exchange on an NMR experiment is the *exchange regime*, which is determined by the rate of chemical exchange (k_{ex}) relative to a relevant spectroscopic quantity, most commonly the frequency difference between states, $\Delta\omega$:

$$\Delta\omega = \gamma B_0 \Delta\delta \tag{12}$$

where γ is the gyromagnetic ratio of the nucleus being observed, B_0 is the static magnetic field strength, and $\Delta\delta$ is the chemical shift difference between the states.

We start by considering the simplest case, in which two exchanging states, A and B, have equal populations. This frequently arises for reasons of symmetry, for example the two methyl groups of dimethylformamide. As described later, the appearance of a 1D spectrum for such a system can be calculated as a function of the exchange rate (Fig. 3A).

When exchange is rapid relative to the frequency difference ($k_{ex} \gg \Delta\omega$, the *fast exchange regime*), a single, sharp resonance will be observed at the average frequency of the two states (Fig. 3A, top). This reflects the molecule jumping between states so rapidly that only a single averaged frequency can be detected.

In contrast, if exchange is slow relative to the frequency difference ($k_{ex} \ll \Delta\omega$, the *slow exchange regime*), then separate, sharp resonances will be observed for each state (Fig. 3A, bottom). This reflects the molecule exchanging between states so slowly that, as far as the NMR experiment is concerned, the two states are chemically completely disconnected. In this situation, the NMR experiment is equivalent to other methods such as UV-vis or fluorescence spectroscopy (because the frequency differences between vibrational or electronic (optical) transitions are many orders of magnitude larger than between NMR transitions).

In between these two limiting cases, the situation becomes more complex as the exchange rate approaches the frequency difference ($k_{ex} \approx \Delta\omega$, the *intermediate exchange regime*) (Fig. 3A). At this point, the two signals observed in the slow exchange regime broaden out until they coalescence into the single resonance observed in the fast exchange regime. For equal populations, this *coalescence point*, defined by vanishing of both first and second derivatives, occurs when $|\Delta\omega| = \sqrt{2}k_{ex}$ [14].

When fast exchange becomes slower and approaches intermediate exchange (the *fast-intermediate exchange regime*), the single resonance that is observed becomes broadened by the effect of chemical exchange, such that its apparent relaxation rate contains an exchange contribution, R_{ex}^{fast} [15]:

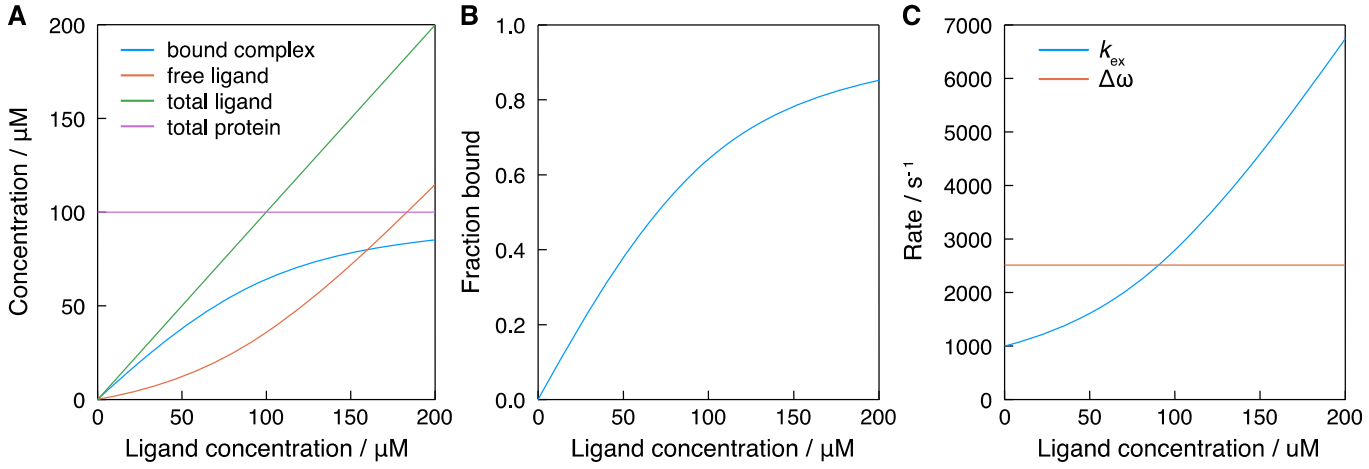

Fig. 2. Illustration of (A) the variation in species concentrations and (B) the fraction of bound protein in a titration as a function of total ligand concentration, and (C) the variation in the exchange rate k_{ex} across the same titration, calculated Eqs. (7) and (11) with K_d = 20 μM, k_{off} = 1000 s^{-1} and $[P]_0$ = 100 μM. The frequency difference $\Delta\omega = \gamma B_0 \Delta\delta$ is also shown as a red line in panel B, calculated for a ^{1}H chemical shift difference of 0.5 ppm at 800 MHz.

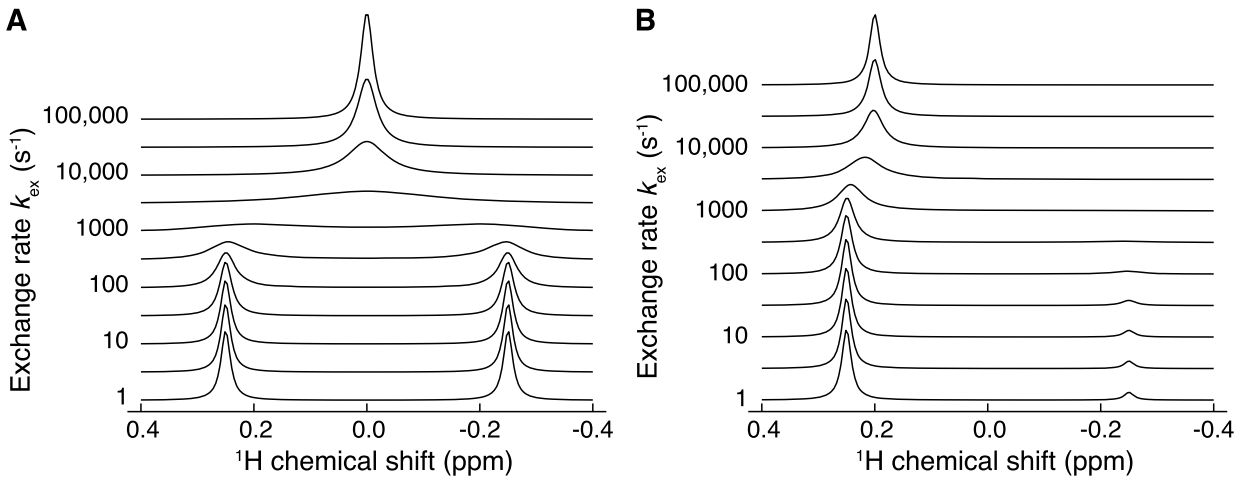

Fig. 3. Resonance line shapes calculated (Eq. 30) for a spin in chemical exchange between two states with a ^{1}H chemical shift difference of 0.5 ppm at 800 MHz ($\Delta\omega = \gamma B_0 \Delta\delta = 2500\ s^{-1}$) and the indicated exchange rate, k_{ex}, for (A) symmetric exchange ($p_A = p_B = 0.5$) and (B) skewed populations ($p_A = 0.9$, $p_B = 0.1$). An interactive workbook is available to explore these simulations further (Supporting Information).

$$R_{ex}^{fast} = \frac{p_A p_B \Delta\omega^2}{k_{ex}} \tag{13}$$

Exchange broadening also leads to a decrease in intensity, which is inversely proportional to the observed linewidth, $R_{2,obs}$ (where $R_{2,0}$ is the linewidth in the absence of exchange processes):

$$R_{2,obs} = R_{2,0} + R_{ex} \tag{14}$$

The expression for R_{ex}^{fast} (Eq. 13) has the same functional form as observed for the low frequency spectral density component of other relaxation processes, e.g. fluctuations in dipole-dipole interactions or chemical shift anisotropy due to rotational diffusion: a mean-square-fluctuation in magnetic field strength ($p_A p_B \Delta\omega^2$) multiplied by the timescale of the fluctuation ($\tau_{ex} = 1/k_{ex}$). Thus, exchange broadening becomes more severe as the chemical shift difference increases or the exchange rate decreases, until the coalescence point is reached.

In the *slow-intermediate exchange regime*, resonances are also broadened by the effect of exchange. In general, the amount of exchange broadening may differ for each state, according to the rate at which the state undergoes chemical exchange (an effect termed lifetime line broadening) [15]:

$$R_{ex}^{slow,A} = k_{AB} \text{ and } R_{ex}^{slow,B} = k_{BA} \tag{15}$$

At the microscopic level, this reflects the additional decay of the free induction decay as spins from a given state undergo stochastic or random exchange that does not add coherently to the magnetisation of the new state.

Unequal populations

The analysis of unequal or highly skewed populations, i.e. when the population of A is significantly larger than B, $p_A \gg p_B$, introduces some additional considerations compared with symmetric exchange, as the behaviour of major and minor states is not equivalent (Fig. 3B). Highly skewed populations can arise in a number of situations, for example in early stages of a titration experiment, macromolecules with sparsely populated intermediate states, or for spins in rapid exchange with the solvent (in this case, the observed spins are the minor state while the solvent is the major state).

For unequal populations in the fast exchange regime, a single resonance is observed at the population-weighted average of the two original states:

$$\omega_{obs} = p_A \omega_A + p_B \omega_B \tag{16}$$

whereas in the slow exchange regime two resonances are observed with population-weighted *amplitudes*. By 'amplitude', we refer to the intensity at the start of the FID, or equivalently the integral of the peak in a simple 1D experiment. We will see shortly that the major and minor state resonances do not generally have the same linewidth, and so measurements of peak intensity alone may not accurately reflect populations of the states.

The expressions presented above for exchange broadening between equally populated states in slow-intermediate and fast-intermediate exchange regimes Eqs. (13) and (15) are also correct for the case of unequal populations. Here we highlight two important consequences of these expressions. Firstly, in the fast-intermediate exchange regime (Eq. 13), even a small population of a minor state can lead to substantial line broadening and loss of signal intensity. Secondly, following our earlier analysis of chemical exchange kinetics, lifetime broadening of a minor state resonance (Eq. 15) is much more severe than for the major state resonance, and so the existence of such resonances may effectively only be detectable indirectly using experiments such as CEST or CPMG relaxation dispersion [19,20].

Exchange between states with different relaxation rates

The discussion above has reviewed the principles of chemical exchange where all states have equal relaxation rates. If this is not the case, then the exchange rate, k_{ex}, should be compared to $|\Delta\omega + i\Delta R_2|$ and not just $\Delta\omega$ [21]. However, as chemical shift differences are typically much greater than differences in relaxation rate, this is usually a very good approximation. Nevertheless, exceptions do arise, for example when small molecules bind to large, rapidly relaxing macromolecules. In such cases, in the fast exchange limit a population-weighted average relaxation rate is observed in addition to an averaged chemical shift, which can be exploited in ligand-observed measurements of binding through relaxation-weighted experiments [9]. Towards the slow exchange limit, the rapidly relaxing state may be difficult to observe directly, but the exchange process, and the rapidly relaxing 'dark' state may still characterised using dark-state exchange saturation transfer (DEST) experiments [22–24].

Modulating the chemical exchange regime

Chemical exchange effects in a spectrum can often present a challenge to analysis – expected peaks may be missing, or broad and poorly resolved, or split into unexpected and confusing multiplets. However, the spectroscopist has a variety of tools available to probe exchange

further in such situations.

Firstly, and perhaps most simply, different atoms within an exchanging system are likely to have different chemical shift differences between states. Therefore, one should not expect all spins to have the same exchange behaviour. This may help to narrow down the possible exchange rates, particularly if different resonances can be observed in both fast and slow regimes [25].

Secondly, the magnetic field strength may be varied to modulate the frequency difference $\Delta\omega$ (Eq. 12) [26]. Changing the field strength will not affect the chemical exchange process itself, but it will affect the observation of the process, analogous to changing the frame rate of a camera. At higher field strengths, exchange will appear to be in a slower regime. In the fast-intermediate regime this can lead to stronger line broadening (Eq. 13), and so a more intense spectrum may in fact be acquired using a lower field spectrometer in order to reduce such line broadening effects.

Thirdly, one can vary the speed of the chemical exchange process by varying the acquisition temperature, in so-called variable temperature (VT) NMR. Both forwards and backwards rates will follow the Arrhenius or Eyring equations and so will depend exponentially on the temperature, and this may be used to shift exchange kinetics to a more favourable regime. The identification of the coalescence point in VT measurements also provides a quick route to determine the exchange rate. However, for unequal populations the relative populations of major and minor states will also vary with temperature according to ΔH and the van't Hoff equation. Therefore, computer simulation tools, discussed further below, are recommended for the quantitative analysis of such data in order to obtain accurately the full breath of information contained in these measurements [27].

Lastly, intermolecular exchange processes can be perturbed by varying the concentrations of components in the reaction. This is most widely appreciated for biomolecular or supramolecular titration measurements, as will be discussed below, but can equally be applied to measurements of small molecules undergoing acid- or base- or solvent-catalysed exchange (and may provide a more accessible method than experimentally complex VT NMR) [28].

Changes in the chemical shift timescale across a titration

A common application of NMR is the analysis of molecular interactions through titration experiments [10,29], and therefore the impact of chemical exchange on these measurements is worth particular comment. As noted above (Eq. 11 and Fig. 2), the exchange rate increases throughout a titration, and therefore the system moves towards faster NMR chemical exchange regimes. This has a number of consequences, which may be observed in the simulated titration measurements shown in Fig 4.

First, in the slow exchange limit, the initial unbound peak has no exchange broadening as there is no exchange in the absence of ligand. In contrast, the bound peak is less intense due to a constant lifetime line broadening, $R_{ex} = k_{off}$ (Eq. 15) (Fig. 4, k_{off} = 10–100 s^{-1}). Lifetime line broadening of the unbound peak within the slow exchange regime varies as $R_{ex} = k_{on}[L]$, i.e. depending on the *free* ligand concentration. If the affinity is high relative to the protein concentration ($[P]_0 \gtrsim K_d[P]_0 \geq K_d$), then the free ligand concentration increases slowly in early stages of the titration and there may be little additional broadening of the unbound peak. However, even a small broadening effect can strongly affect measurements of peak intensity, such that they are no longer proportional to the unbound concentration (Fig. 4, k_{off} = 100 s^{-1}). In contrast, if the affinity is low or the association rate is rapid, then line broadening of the unbound resonance at early stages of a titration can be particularly severe as exchange approaches the intermediate exchange regime (Fig. 4, k_{off} = 1000 s^{-1}).

Towards the fast exchange limit (Fig. 4, $k_{off} \geq$ 10,000 s^{-1}), the observed chemical shift perturbation is a good approximation to the fraction bound. However, where initial stages of the titration are in the slow or intermediate exchange regimes (Fig. 4, k_{off} = 1000 s^{-1}), chemical shift perturbations will initially be small and their analysis will not provide an accurate measure of binding [29]. Exchange broadening is apparent even for extremely rapid dissociation rates. Ultimately, Fig. 4 demonstrates the sensitivity of NMR spectra to exchange rates varying across four orders of magnitude, and by implication also indicates the capacity to analysis such processes using techniques such as line shape analysis.

Lastly, lifetime line broadening of the bound state in slow exchange can be eliminated by the addition of an excess of ligand to push the exchange rate into the fast exchange regime (Fig. 5). This results in the *backwards* movement of the bound resonance from the bound chemical shift towards the population-weighted average of free and bound chemical shifts expected in fast exchange (Eq. 16). On addition of further

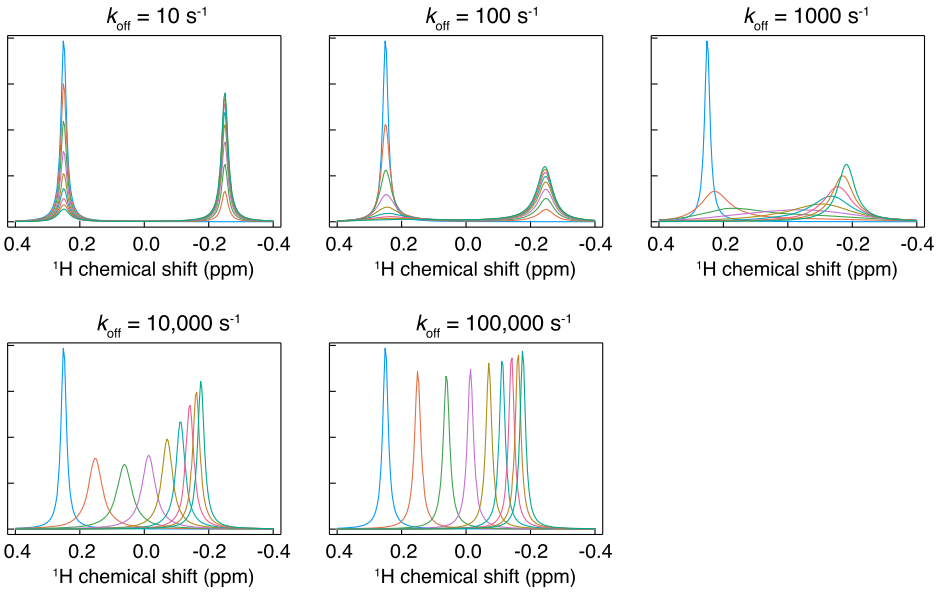

Fig. 4. Simulated resonance line shapes across a titration experiment, calculated following Eqs. (7), (11) and (30), matching conditions shown in Fig. 2 (δ_P -0.25 ppm, δ_{PL} 0.25 ppm, 800 MHz, K_d 20 μM, protein concentration 100 μM, ligand concentrations 0, 25, …, 200 μM). An interactive workbook is available to explore these simulations further (Supporting Information).

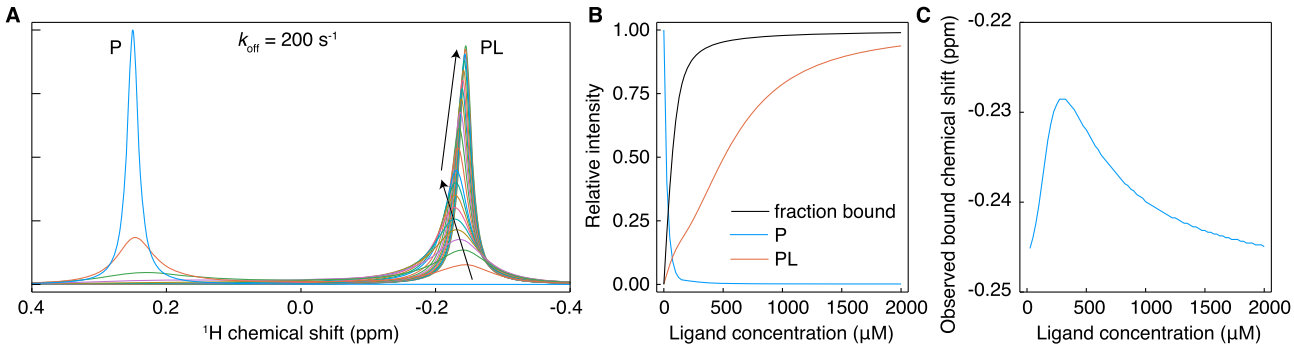

Fig. 5. Impact of the transition between slow and fast exchange regimes at late stages of a titration. (A) Simulation of a titration measurement, calculated as in Fig. 4, with $k_{off} = 200\ s^{-1}$ and ligand concentrations increasing up to 2 mM (20 equiv). (B) Variation in apparent resonance intensities, and (C) the observed chemical shift of the bound resonance.

ligand to saturate binding, the resonance then shifts again towards the bound chemical shift (Fig. 5C).

Multi-dimensional NMR experiments

Chemical exchange in multi-dimensional (and often heteronuclear) experiments brings some new considerations [30–32]. Firstly, the impact of exchange broadening on resonance intensities is more severe. While resonance intensities in one-dimensional spectra are strongly affected by exchange, their integrals can still be expected to provide a quantitative measure of population. However, in multi-dimensional experiments, exchange-induced relaxation results in a loss of signal during coherence transfer periods (CTPs) such that peak integrals may no longer be quantitative. Moreover, because cross-peak intensities are inversely proportional to the product of linewidths in all dimensions they are more strongly attenuated by chemical exchange, e.g. for direct and indirect dimensions of a two-dimensional experiment:

$$I = I_0 \cdot (\text{relaxation loss during CTPs}) \cdot \frac{1}{R_{2,0}^{\text{direct}} + R_{ex}^{\text{direct}}} \cdot \frac{1}{R_{2,0}^{\text{indirect}} + R_{ex}^{\text{indirect}}} \qquad (17)$$

Secondly, defining the exchange regime is more complicated for two-dimensional experiments, because the appearance of the resonances depends on frequency differences in both direct and indirect dimensions. Thus, depending on the relative magnitudes of these, chemical exchange may appear fast in one dimension but slow in the other [32].

Thirdly, the effect of chemical exchange on a 2D spectrum depends on the NMR experiment itself [30]. In HSQC and (amide) TROSY experiments [33,34], magnetisation is single-quantum during the indirect evolution period, and so the exchange rate should be compared with the indirect frequency difference, $\Delta\omega_S$, to determine the exchange regime. However, in the HMQC experiment [35] (commonly used as the SOFAST-HMQC variant [36], or for methyl TROSY measurements [37]), magnetisation is exchanged between zero- and double-quantum coherences during the indirect evolution period. Thus, the exchange rate should be compared with both the zero-quantum frequency difference, $\Delta\omega_{ZQ} = \Delta\omega_S - \Delta\omega_I$, and the double-quantum frequency difference, $\Delta\omega_{DQ} = \Delta\omega_S + \Delta\omega_I$, to understand the relevant chemical exchange regime in the indirect dimension. 'Fast exchange' behaviour of 2D resonances will only be observed when exchange is fast with respect to all three of $\Delta\omega_I$, $\Delta\omega_{ZQ}$ and $\Delta\omega_{DQ}$ [32]. This is a smaller region of $(\Delta\omega_I, \Delta\omega_S)$ parameter space than for a single quantum correlation experiment, with the practical consequence that during titrations it is likely to be easier to follow progressive chemical shift changes using HSQC experiments than HMQC experiments. Moreover, in some slow exchange regimes the direction of chemical shift perturbations can be the reverse of that ordinarily expected, with resonances moving *away* from each other as the titration progresses. This is discussed in more detail in reference [32].

Lastly, chemical shift evolution in multiple dimensions is not necessarily independent. Instead, exchange can give rise to unexpected cross-peaks with complex structure and distorted phases in even the simplest 2D spectra, including COSY, NOESY and heteronuclear HSQC and HMQC experiments [31]. Some illustrative examples are provided for the symmetric exchange of methyl groups in the simple molecule N, N-dimethyltrichloroacetamide (Fig. 6), which occurs on a timescale of 125 s^{-1} at 298 K [26,38].

In summary, despite their apparent simplicity, 2D NMR experiments can depend on chemical exchange in complex ways. Naïve analysis of chemical shift perturbations or intensities can risk introducing systematic errors into results. However, as will be discussed below, 2D experiments are also amenable to computer line shape analysis [30], and their high sensitivity to exchange effects means that they have the potential to provide rich kinetic and mechanistic information on molecular interactions.

One-dimensional lineshape analysis

Principles

Previous sections have described the ways in which chemical exchange can influence the appearance of an NMR spectrum. As shown in the examples above, NMR spectra can be accurately simulated for a given set of parameters, representing both spectroscopic and kinetic aspects of the system (i.e. chemical shifts, relaxation rates, equilibrium constants and exchange rates). The details of these calculations are described in the following section, and from here it is a relatively straightforward matter to couple these simulations to a fitting algorithm in order to estimate the best-fitting parameters from a collection of observed spectra, in a procedure referred to as *lineshape analysis* or *dynamic NMR* [39,40].

Lineshape analysis provides dynamic information from simple and sensitive one-dimensional experiments. We have seen earlier that line shapes are sensitive to exchange rates across four orders of magnitude (Fig. 7) – ca. 50x above and below the frequency difference $\Delta\omega$. Analysis of multiple spins, with different chemical shift differences, can extend this range further, resulting in sensitivity to exchange rates from ca. 10 to 250,000 s^{-1} (estimated for ^{1}H chemical shift differences between 0.1 and 1 ppm at 800 MHz). Beyond this, variable temperature NMR can also be employed to shift processes into a suitable timescale for lineshape analysis.

In the presence of chemical exchange, resonance linewidths are given by Eq. (14). In some cases, particularly for small molecules, exchange broadening may be so strong that the contribution from ordinary relaxation can be neglected. In general, however, to accurately separate kinetic effects from ordinary relaxation processes, some form of external perturbation is required to modify the exchange terms specifically. This may be via a series of spectra acquired across a titration, or through variable temperature NMR in which equilibrium concentrations may be

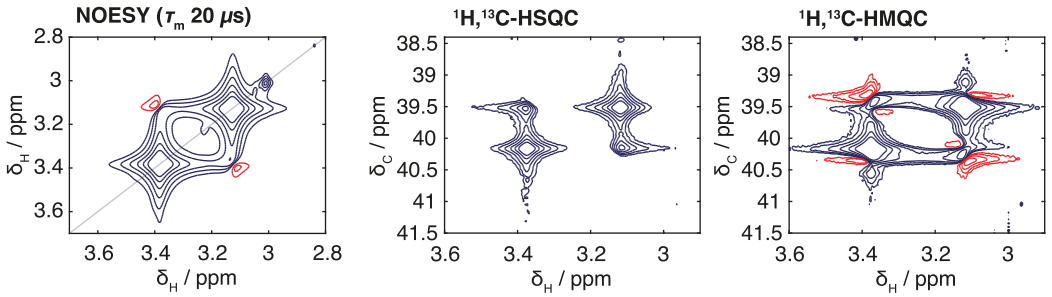

Fig. 6. Observation of exchange cross-peaks in simple homonuclear and heteronuclear two-dimensional NMR spectra of methyl groups in the small molecule N,N-dimethyltrichloroacetamide (DMTCA), acquired at 16.44 T, 298 K (k_{ex} 125 s^{-1}) [adapted from [31]].

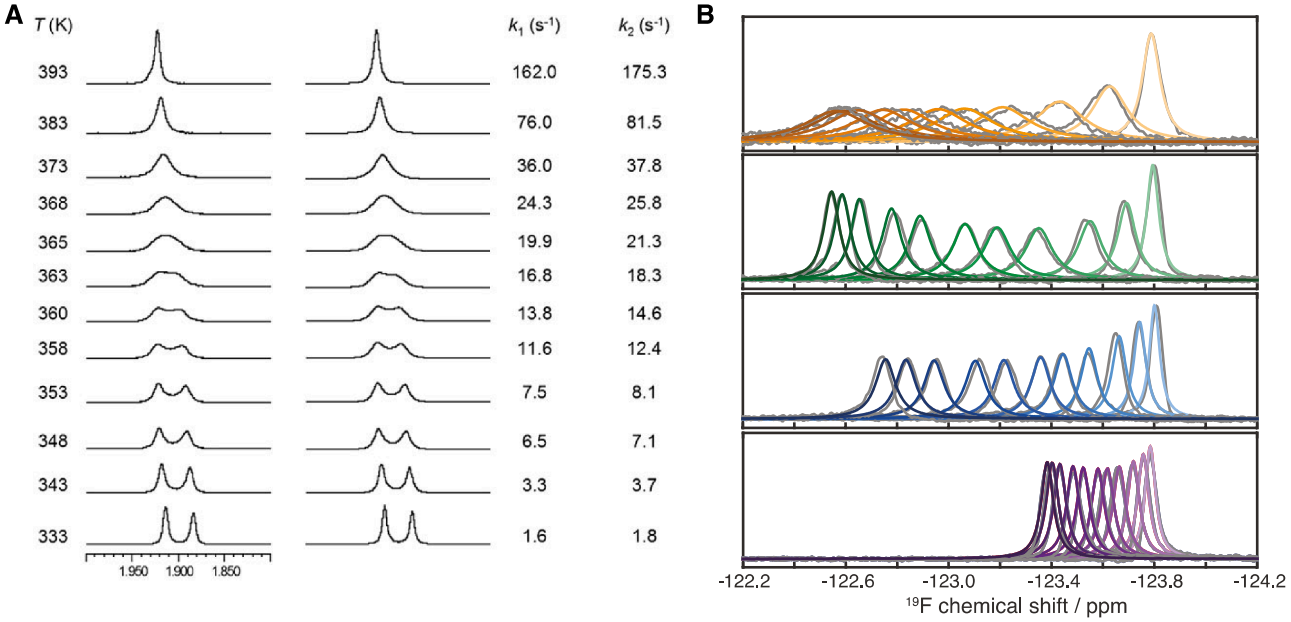

Fig. 7. Examples of one-dimensional lineshape analysis. (A) Lineshape analysis of *cis/trans* isomerisation in a peptoid by VT NMR [adapted from [27]]. Experimental spectra are shown on the left, and simulated spectra on the right alongside forwards and backwards rate constants, fitting using gNMR [41]. (B) ^{19}F lineshape analysis of the titration of four unlabelled peptides binding to an SH3 domain labelled with 5-fluorotryptophan [adapted from [42]]. Observed data are shown in grey, and simulated spectra in colour, fitting by direct calculation in MATLAB .

fit to the Van't Hoff equation and exchange rates to Arrhenius or Eyring equations.

Some examples of lineshape analysis are presented in Fig. 7. Lineshape analysis can also provide sensitivity to more complex interaction mechanisms, for example identifying and distinguishing induced fit or conformational selection mechanisms [11,18,43].

Calculation methods

In this section, we will outline the analysis of chemical exchange for a spin undergoing chemical exchange between two states, A and B. We will assume that the spin is uncoupled, so that its evolution may be described in classical terms using the vector model, via the Bloch-McConnell equations [44]. However, the extension to coupled systems is relatively straightforward [39,45].

The time-evolution of magnetisation for a single state can be described by the Bloch equations:

$$\frac{d}{dt}\begin{pmatrix} M_x \\ M_y \\ M_z \end{pmatrix} = -\begin{pmatrix} R_2 & \omega_0 & -\omega_y \\ -\omega_0 & R_2 & \omega_x \\ \omega_y & -\omega_x & R_1 \end{pmatrix} \cdot \begin{pmatrix} M_x \\ M_y \\ M_z \end{pmatrix} + \begin{pmatrix} 0 \\ 0 \\ R_1 M_0 \end{pmatrix} \tag{18}$$

where ω_0 is the Larmor frequency, ω_x and ω_y are the B_1 field strengths (i.e. rf pulses), and M_0 is the total magnetisation at equilibrium. We are generally interested in the analysis of exchange under free evolution, such that $\omega_x = \omega_y = 0$. As transverse relaxation is also generally much more rapid than longitudinal relaxation, we can focus only on the *xy*-plane, such that Eq. (18) therefore simplifies to:

$$\frac{d}{dt}\begin{pmatrix} M_x \\ M_y \end{pmatrix} = -\begin{pmatrix} R_2 & \omega_0 \\ -\omega_0 & R_2 \end{pmatrix} \cdot \begin{pmatrix} M_x \\ M_y \end{pmatrix} \tag{19}$$

Combining *x* and *y* components as a single complex number in the *xy*-plane, $M_{xy} = M_x + iM_y$, we have:

$$\frac{dM_{xy}}{dt} = (i\omega_0 - R_2)M_{xy} \tag{20}$$

which is solved by:

$$M_{xy}(t) = e^{(i\omega_0 - R_2)t} M_{xy}(0) \tag{21}$$

Let us now consider the evolution of transverse magnetisation for two species, that do not undergo chemical exchange, which can be written compactly in matrix form:

$$\frac{d}{dt}\begin{pmatrix} M_A \\ M_B \end{pmatrix} = \begin{pmatrix} i\omega_A - R_{2,A} & 0 \\ 0 & i\omega_B - R_{2,B} \end{pmatrix} \cdot \begin{pmatrix} M_A \\ M_B \end{pmatrix} \tag{22}$$

or equivalently

$$\frac{d\vec{M}}{dt} = (i\Omega - R)\cdot\vec{M} \tag{23}$$

where $\Omega = \begin{pmatrix} i\omega_A & 0 \\ 0 & i\omega_B \end{pmatrix}$ and $R = \begin{pmatrix} R_{2,A} & 0 \\ 0 & R_{2,B} \end{pmatrix}$ are diagonal matrices representing chemical shifts and relaxation rates. In analogy with Eq. (21), the solution to Eq. (23) can be written compactly as a matrix exponential:

$$\vec{M}(t) = e^{(i\Omega - R)t}\vec{M}(0) = e^{Lt}\vec{M}(0) \tag{24}$$

where the initial magnetisation $\vec{M}(0)$ is proportional to the equilibrium concentrations of species and the operator $L = i\Omega - R$. By its definition, L is diagonal and the frequencies and linewidths of observed resonances correspond to the imaginary and real components of its eigenvalues. However, the presence of chemical exchange introduces an exchange operator, K, that couples together exchanging species (Eq. 9):

$$L = i\Omega - R + K \tag{25}$$

The observed magnetisation is then the sum of individual components:

$$M_{obs}(t) = M_A(t) + M_B(t) = (\,1 \quad 1 \quad \cdots\,)\, e^{Lt}\,\vec{M}(0) \tag{26}$$

The free induction decay may be calculated directly from Eq. (26), from which the frequency domain spectrum can be obtained in the usual manner by Fourier transformation. Alternatively, L can be diagonalised as $Q\Lambda Q^{-1}$, where Λ is a diagonal matrix of eigenvalues, such that $e^{Lt} = Qe^{\Lambda t}Q^{-1}$ and the observed magnetisation is:

$$M_{obs}(t) = (\,1 \quad 1 \quad \cdots\,)\, Qe^{\Lambda t}Q^{-1}\,\vec{M}(0) \tag{27}$$

As before, the eigenvalues of L, $\{\lambda_1, \lambda_2, \ldots\}$, describe the frequencies and linewidths of the observed resonances [40]. Nothing that $e^{\Lambda t} = \mathrm{diag}(e^{\lambda_1 t}, e^{\lambda_2 t}, \ldots)$ is the only term depending on time, an analytic expression for the frequency domain spectrum can then be obtained by Fourier transform of Eq. (27):

$$Y(\omega) = (\,1 \quad 1 \quad \cdots\,)\, Q\, F\left[e^{\Lambda t}\right]\, Q^{-1}\,\vec{M}(0) \tag{28}$$

where the Fourier transforms of exponentials are Lorentzians:

$$F\left[e^{\Lambda t}\right] = \mathrm{diag}\left(\frac{1}{\lambda_1 - i\omega}, \frac{1}{\lambda_2 - i\omega}, \ldots\right) \tag{29}$$

This expression can be calculated efficiently numerically and integrated into a nonlinear minimisation algorithm to fit experimental data [40,46]. For the case of two-state exchange, an analytical expression for the observed spectrum can also be derived by this approach [47–49]:

$$Y(\omega) = \frac{k_{ex} + p_A\left(R_{2,B} - i[\omega - \omega_B]\right) + p_B\left(R_{2,A} - i[\omega - \omega_A]\right)}{k_{ex}p_A\left(R_{2,A} - i[\omega - \omega_A]\right) + k_{ex}p_B\left(R_{2,B} - i[\omega - \omega_B]\right) + \left(R_{2,A} - i[\omega - \omega_A]\right)\left(R_{2,B} - i[\omega - \omega_B]\right)} \tag{30}$$

Further analytical expressions have also been derived for more complex exchange models [48].

Data acquisition

The acquisition of one-dimensional experiments for analysis is usually straightforward. Nevertheless, care should be taken to ensure accurate sample concentrations, particularly across a titration series; to have well-shimmed samples with as little inhomogeneous broadening as possible; to have a flat baseline, with good quality solvent suppression if required; and to use the same acquisition parameters, such as spectral width and time domain size, across all experiments. For variable temperature measurements, accurate sample temperatures should be determined using an external reference such as d4-methanol [50]. Lastly, if multiple spectra are being fitted simultaneously, it is important that pulses are calibrated to ensure consistent excitation, and that sufficiently long recycle delays are employed to ensure complete relaxation between scans.

Software

A variety of software packages have been developed that provide graphical interfaces for one-dimensional lineshape analysis, summarised in Table 1. As shown, these packages each provide varying degrees of useability and compatibility with different operating systems, and the capacity to simulate and fit scalar coupled spin systems, overlapping resonances, multi-state exchange mechanisms, and multiple spectra associated with titration measurements. As this table shows, no single package is available that handles the variety of different requirements fully. For this reason, and given the relative simplicity of calculations, one-dimensional lineshape analysis is also commonly performed using home-written scripts or analysis routines [11,42,51,52]. This may permit, for example, the analysis of titration measurements across multiple temperatures [53], integration with CEST measurements [52], or the analysis of multi-state binding mechanisms [11,53].

Two-dimensional lineshape analysis

Principles

The principles of lineshape analysis can be extended from one-dimensional experiments to the two-dimensional experiments common in biomolecular NMR [30,60]. While, as noted earlier, the effects of chemical exchange on multi-dimensional and particularly heteronuclear experiments can be more complicated than simple one-dimensional experiments, they can provide both increased residue specificity and resolution, together with greater sensitivity to the effects of exchange.

In contrast to the analysis of relatively simple one-dimensional experiments, the analysis of two-dimensional experiments can be implemented using a 'virtual spectrometer', which reproduces the specific details of the pulse program that was used experimentally (Fig. 8).

Calculation methods

Two-dimensional spectra can be simulated by the direct propagation of magnetisation within a composite Liouville space formed from the direct product of an N-dimensional chemical state space and a Liouville space or subspace describing the required spin operators [30,62]. While the calculation may be more elaborate, the fundamental principles of it are similar to the simulation of one-dimensional experiments in the presence of scalar couplings [39,45].

For a two-spin system such as an amide group, the spin Liouville space is 16-dimensional, and so for N chemical states the composite space would be $16N$-dimensional. However, while simulations can be

Table 1
Summary of software packages available for one-dimensional lineshape analysis.

Software	Platform	NMRBox	Multiple spectra	Fit overlapping resonances	Scalar coupling	Exchange mechanisms	Comments	Ref
NmrLineGuru	Windows, Linux	Yes	Yes (titration data)	No	No	Limited (ligand binding, induced fit, two-site ligand binding)	Simple interface; designed for biomolecular NMR	[54]
Topspin (dnmr)	Windows, Mac, Linux	Yes	No	Yes	Yes	General	Integrated with data processing	[55]
gNMR	Windows, Mac	No	No	Yes	Yes	General		[41]
iNMR	Mac	No	No	Yes	Yes	General	Integrated with data processing	[56]
WinDNMR	Windows	No	No	Yes	Yes	General		[57, 58]
SpinWorks	Windows	No	No	Yes	Yes	Two-state	Integrated with data processing	[40, 59]

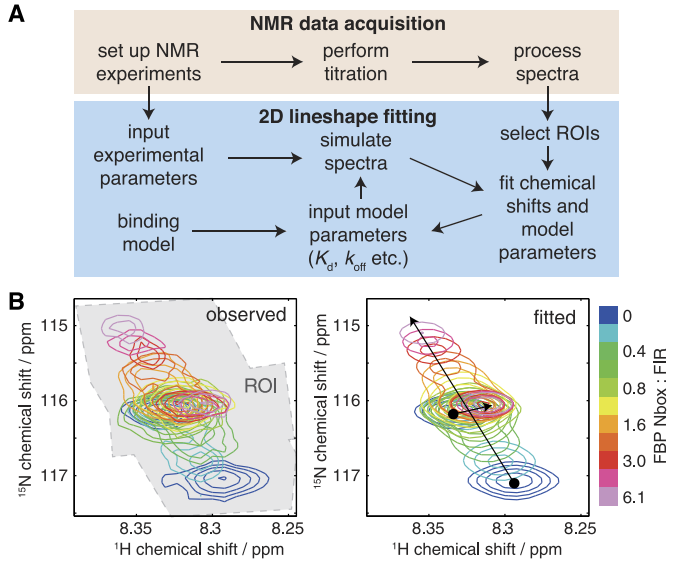

Fig. 8. (A) Principles of 2D lineshape analysis [reproduced from [30]]. Outline of the data acquisition process and the two-dimensional lineshape analysis procedure. ROI (region of interest) indicates regions of the observed spectra selected for use in the fitting, typically enclosing one or more residues whose appearance varies across the titration series. (B) 2D lineshape analysis of the interaction of FIR RRM1-RRM2 with the FBP Nbox peptide using NMR TITAN [30]. Observed and fitted ^{1}H,^{15}N SOFAST-HMQC spectra are shown for 41μM FIR RRM1-RRM2 upon titration of FBP Nbox [61].

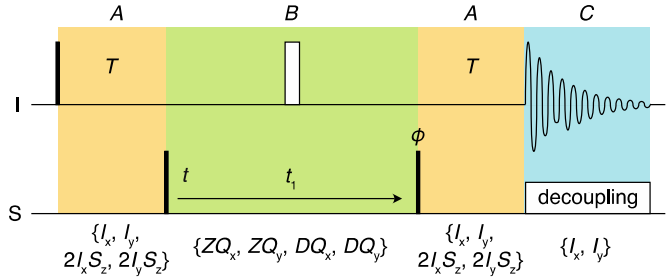

Fig. 9. The HMQC pulse sequence. Sections of the sequence are coloured and marked (A, B, C) according to the Liouville subspace used for two-dimensional lineshape calculations (shown underneath) [30]. The delay $T = 1/2J_{IS}$. Solid bars indicate 90° pulses and hollow bars 180° pulses, applied with phase x. The pulse marked φ is applied with phases x and y for quadrature detection. The operators $ZQ_{x/y} = I_{x/y}S_x \pm I_{y/x}S_y$ and $DQ_{x/y} = I_xS_{x/y} \mp I_yS_{y/x}$.

carried out in this complete basis [62], it is generally desirable to carry out calculations in a reduced basis, eliminating coherences that are not accessed by the pulse program, and neglecting cross-correlated relaxation processes and longitudinal relaxation. This serves two purposes. First, reducing matrix sizes greatly accelerates numerical calculations. Second, these approximations reflect the limited information that is available when fitting a spectrum. In general, one can only hope to determine a linewidth and chemical shift from each dimension for a given resonance, and so it is not helpful to include additional longitudinal or cross-correlated relaxation rates as free parameters.

The specifics of a calculation depend on the particular details of the pulse program being simulated. These have been reported previously [30–32], so here we provide a single, detailed example for an HMQC experiment (Fig. 9).

The initial populations of states, p_0, are determined from analysis of the chemical equilibrium model, comprising N states. From this, an initial density operator, ρ_0 (following the first 90° pulse), is determined, proportional to $-I_y$:

$$\rho_0 = p_0 \otimes \begin{pmatrix} 0 & -1 & 0 & 0 \end{pmatrix}' \tag{31}$$

Here $\otimes$ indicates the Kronecker product between the space of chemical states and the Liouville (sub)space of density operators. During period A, coherences evolve under the operator L_A,

$$L_A = \bigoplus_{i=1}^{N} \begin{pmatrix} -R^I_{2,i} & -\omega^I_i & 0 & -\pi J \\ \omega^I_i & -R^I_{2,i} & \pi J & 0 \\ 0 & -\pi J & -R^I_{2,i} & -\omega^I_i \\ \pi J & 0 & \omega^I_i & -R^I_{2,i} \end{pmatrix} + K \otimes I_4 \tag{32}$$

such that at the end of period A, the density operator is $\rho_A = e^{L_A T}\rho_0$. At this point, we may apply the 90° S pulse and change basis from A to B using the matrix R_{AB},

$$R_{AB} = \frac{1}{2} I_N \otimes \begin{pmatrix} 0 & 0 & 0 & -1 \\ 0 & 0 & -1 & 0 \\ 0 & 0 & 0 & 1 \\ 0 & 0 & -1 & 0 \end{pmatrix} \tag{33}$$

to obtain $\rho_{B,0} = R_{AB}\rho_A$. Zero and double quantum coherences then evolve for time $t_1/2$ under the influence of L_B,

$$L_B = \bigoplus_{i=1}^{N} \begin{pmatrix} -R^S_{2,i} & \omega^I_i - \omega^S_i & 0 & 0 \\ -\omega^I_i + \omega^S_i & -R^S_{2,i} & 0 & 0 \\ 0 & 0 & -R^S_{2,i} & -\omega^I_i - \omega^S_i \\ 0 & 0 & \omega^I_i + \omega^S_i & -R^S_{2,i} \end{pmatrix} + K \otimes I_4 \tag{34}$$

Following this, the central 180° pulse interchanges zero and double quantum coherences, according to the propagator U_{180},

$$U_{180} = I_N \otimes \begin{pmatrix} 0 & 0 & 1 & 0 \\ 0 & 0 & 0 & 1 \\ 1 & 0 & 0 & 0 \\ 0 & 1 & 0 & 0 \end{pmatrix} \tag{35}$$

following which a further period of free precession occurs for time $t_1/2$, resulting in the density operator at the end of period B, $\rho_B = e^{L_B t_1/2} U_{180} e^{L_B t_1/2} \rho_{B,0}$. This can then be rotated back into the basis A following application of the second 90° S pulse. This transformation depends on the phase of the pulse, ϕ, and can be described by the two matrices R^x_{BA} and R^y_{BA},

$$R^x_{BA} = I_N \otimes \begin{pmatrix} 0 & 0 & 0 & 0 \\ 0 & 0 & 0 & 0 \\ 0 & 1 & 0 & 1 \\ 1 & 0 & -1 & 0 \end{pmatrix} \tag{36}$$

and

$$R^y_{BA} = I_N \otimes \begin{pmatrix} 0 & 0 & 0 & 0 \\ 0 & 0 & 0 & 0 \\ -1 & 0 & -1 & 0 \\ 0 & 1 & 0 & -1 \end{pmatrix} \tag{37}$$

Following a further period of free evolution under the operator L_A, magnetisation is detected by projection onto $I^- = I_x - iI_y$,

$$I^- = p'_0 \otimes (1 \quad -i \quad 0 \quad 0) \tag{38}$$

So that the observed magnetisation at the start of period C is:

$$M^{x/y}_{\text{obs}} = < I^- e^{L_A T} R^{x/y}_{BA} e^{L_B t_1/2} U_{180} e^{L_B t_1/2} R_{AB} e^{L_A T} \rho_0 > \tag{39}$$

Thus, two terms are calculated, corresponding to cosine and sine-modulated signals in the indirect dimension. This magnetisation can then be used as input, $\vec{M}(0)$, for calculation of lineshapes in the direct dimension according to the Bloch-McConnell equations (Eq. 28). Finally, window functions can be applied to the indirect dimension and Fourier transformed to yield the required two-dimensional simulated spectrum for the spin system (i.e. for a single residue). This procedure is then repeated for each spin system being simulated.

Regions of simulated spectra can be extracted that correspond to experimental regions of interest, and optimised using a least squares fitting algorithm. Typically, one or two dozen residues are simulated for the analysis of macromolecules, and their amplitudes (overall intensities) at each point in the fitting procedure are optimised by linear regression against the observed spectra. Importantly, because the pulse sequence is simulated in its entirety, amplitudes can be fixed across series of titration points, after scaling for varying numbers of scans or receiver gain. Changes in intensity can therefore provide important constraints on unknown parameters, while residues that overlap strongly during part of the titration can be treated easily (Fig. 8B).

Data acquisition

Practical aspects of data acquisition for two-dimensional lineshape analysis have been reviewed recently [60]. Here, we summarise some key points. Many of the aspects discussed earlier for one-dimensional experiments apply equally to two-dimensional lineshape analysis. However, the coding of the pulse program is more critical for two-dimensional measurements, to ensure good quality baselines and phasing in the indirect dimension through initial zero- or half-dwell delays in the evolution time. Suitable sequences (in Bruker format) are included within the NMR TITAN analysis package (www.nmr-titan.com). Sufficiently long acquisition times should be chosen so that relaxation can be observed within the free induction decay (particularly relevant to the indirect dimension), to ensure accurate estimates can be made of resonance linewidths when transformed into the frequency domain. Again, consistent acquisition parameters must be used across all spectra in a titration series. Current analysis software also requires that spectra are processed using exponential window functions so that signals retain their Lorentzian profile (this is not a fundamental requirement, but practically acts to accelerate calculations).

As discussed above, different two-dimensional experiments are associated with the evolution of different coherences in the indirect dimension, and this changes the impact of chemical exchange on the observed resonances [30]. In particular, HMQC experiments are more subject to exchange-induced broadening than HSQC experiments [32]. This is not necessarily negative, as this broadening contains useful information on the exchange process, but equally it may prove easier to follow peak movements within HSQC spectra. We have recently described a new SOFAST-H(Z/D)QC experiment for the simultaneous acquisition of HZQC (heteronuclear zero quantum coherence) and HDQC (heteronuclear double quantum coherence) experiments, applicable both to amide and methyl spin systems with optional longitudinal-relaxation enhancement [32]. As the acquisition of these experiments can be rapid relative to sample preparation and calibration, experimentalists may wish to consider acquisition using multiple pulse sequences. These measurements can then be analysed independently, to provide additional confidence in the fitted parameters [32].

Two common pulse sequences that pose difficulties for two-dimensional lineshape analysis are the sensitivity-enhanced HSQC [63], and (amide) TROSY [34]. This is due to the more complex coherence transfer steps within the experiments, involving several different coherences (e.g. multiple quantum and longitudinal coherences) that cannot be estimated from the observed spectra. To the extent that relaxation and exchange can be neglected during coherence transfer periods, data acquired with these sequences may be analysed, but in general it is preferable to use other sequences. One such alternative is the ZQ-TROSY experiment [64], also available as a longitudinal-relaxation enhanced BEST-ZQ-TROSY variant [32], which correlates the ^{1}H TROSY line with the zero-quantum coherence. This is expected to have a relaxation rate between that of ^{15}N single-quantum and ^{15}N TROSY coherences, and so the experiment may provide a useful alternative to standard TROSY that remains amenable to two-dimensional lineshape analysis [32].

A final point to consider for data acquisition is the use of longitudinal-relaxation enhanced experiments such as the SOFAST-HMQC [36] or BEST experiments [65] (note that acquisition of so-called ultrafast experiments, using single-scan spatial encoding methods, is not recommended due to their complex or distorted lineshapes [66]). These can allow greatly increased sensitivity and/or more rapid acquisition, making their use particularly favourable for titration studies. However, the intensity of resonances in these spectra is strongly dependent on their longitudinal relaxation rate, R_1 (or more accurately, on the effective longitudinal relaxation rate accounting for selective excitation). Where there is a difference, ΔR_1, between states, the effect of chemical exchange should also be considered. As longitudinal relaxation is slow, we can expect that $\Delta R_1 \ll k_{\text{ex}}$ (akin to the fast exchange of transverse relaxation discussed above), and so the observed relaxation rate is a population-weighted average of the individual relaxation rates. As this may shift along the course of a titration experiment, the impact on spectra of strong longitudinal relaxation weighting may need to be considered. However, practically, provided that an excessively short recycle delay is avoided for these experiments, it is our experience that no ill effects are observed from their use (e.g. when compared with independent biophysical measurements of binding affinities [30,32]), but that the increased sensitivity is instead useful for obtaining high-quality spectra within a shorter period of time.

Software

In contrast to the variety of software that has been developed for one-dimensional lineshape analysis, few packages are available for two-dimensional lineshape analysis. NMRKIN [67] and LineShapeKin [18] are capable of performing analysis on one-dimensional cross-sections from two-dimensional spectra. However, as described above, such analyses cannot account for the full complexity of two-dimensional experiments: multiple-quantum evolution, differential relaxation, or exchange cross-peaks. Therefore, their use is not recommended. Only one package, NMR TITAN (www.nmr-titan.com), is currently available for full two-dimensional lineshape analysis [30]. The package, also available on the NMRBox platform [68], provides a simple user interface and permits analysis of a variety of binding mechanisms and pulse programs, including NOESY, HSQC, HMQC, HZQC and HDQC experiments. Its use has been reviewed in a recent article [60], and has now been applied to a variety of systems [69–75]. We draw the interested reader's attention to the discussion of analysis workflows, and the optimal selection of spin systems and regions of interest, that is presented in this article [60].

NMR TITAN provides three methods for the estimation of parameter uncertainty. The first of these is simply the uncertainty derived from the curvature of the χ^2 surface (sum of squares of residuals) as a function of parameters, which is readily obtained as part of the least-squares optimisation algorithm. However, it is our experience that these uncertainties are usually underestimates that may reflect local minima within the χ^2 surface, neglecting the effect of correlations in data that arise through the apodization and Fourier transform of time-domain observations. Therefore, two additional algorithms have been implemented. The first of these is a block residual resampling algorithm [76], in which a large number of bootstrap replicas are constructed by resampling residuals from the original fit, and then re-fitted to determine the distribution of parameter estimates. Small tiles of neighbouring points are resampled in this approach to preserve the correlation structure of the observations – if this is neglected, we have found that uncertainties are underestimated [30]. This can determine standard errors for parameter estimates, but may also reveal the presence of highly correlated parameters which may warrant manual inspection and consideration. The final approach is a leave-one-out jackknife, in which spin systems are systematically omitted from fits to determine a distribution of parameter estimates. This is particularly effective at revealing strong dependencies on a single resonance and may indicate that additional spin systems should be included to increase the robustness of the analysis. Ultimately, we recommend that all error analyses should be performed, and to be conservative it is the largest uncertainties that should be reported.

Conclusions

NMR spectra of all kinds can carry valuable imprints of chemical exchange phenomena. Lineshape analysis, or dynamic NMR, provides a rigorous theoretical approach for the analysis of such effects, that can complement analyses by other NMR methods such as EXSY [77], CEST [19] or CPMG relaxation dispersion [20], as well as other biophysical techniques to probe molecular interactions. By introducing the background and fundamental principles of these methods, as well as a detailed description of the underlying calculations, it is hoped that this article might inspire or support others, across many fields of solution NMR spectroscopy, to more fully utilise this powerful analytical method.

By this stage, the fundamental principles of lineshape analysis are well established. However, despite the apparent maturity of the technique, there is much that remains to be developed. Surprisingly, given the long history of 1D analysis, there is no software package capable of performing a full range of analyses (Table 1). Practically therefore, if these methods are to transition from a specialised analysis technique to a commonly used tool, there is a need to develop software presenting a simple graphical interface – as developed for 2D lineshape analysis – that avoids need for users to have expertise in scripting and coding.

Looking ahead, there are opportunities to transfer techniques developed for two-dimensional lineshape analysis to one-dimensional experiments. Practically, many one-dimensional experiments are not simply pulse-acquire sequences, as is implicit in expressions derived for lineshapes (Eq. 30), but they may contain additional evolution periods for solvent suppression during which exchange can occur and scalar couplings may evolve. More generally, there is a need for deeper integration of lineshape analysis with other methods, both spectroscopic and biophysical. As an example of this, we have recently demonstrated the simultaneous analysis of one-dimensional ^{19}F lineshapes and ^{19}F CEST measurements, enabling characterisation of co-translational folding equilibria within large, low concentration and unstable ribosome-nascent chain complexes [52]. A key statistical challenge to address is the accurate determination of parameter uncertainties, from large scale and non-linear fitting procedures, and correctly identifying the most appropriate mechanistic model of chemical exchange that accounts for available data, although progress has been made here in the use of Bayesian analysis techniques [78]. Lineshape fitting methods can also be applied to parametric estimation problems separate from chemical exchange, for example in the analysis of methyl side-chain dynamics by fitting ^{1}H-coupled ^{13}C multiplets to determine cross-correlated relaxation rates [79]. There is the potential for these methods to be coupled with automated, optimal acquisition protocols [80], and for the application of machine learning methods to accelerate the interpretation of NMR observations [81]. Thus, we are confident that this technique has a bright future that will find increasing applications across a variety of chemical and biological systems.

Supporting Information

Interactive workbooks for the exploration of chemical exchange in one-dimensional spectra (Fig. 3 and 4) are available at https://github.com/waudbygroup/pluto-nmr-workbooks.

Declaration of Competing Interest

The authors declare that they have no known competing financial interests or personal relationships that could have appeared to influence the work reported in this paper.

Data availability

No data was used for the research described in the article.

Acknowledgements

We acknowledge financial support from the Spanish Ministry of Science and Innovation and Spanish Research Agency (PID2021-128411NB-I00, MCI/AEI/10.13039/501100011033, FEDER/EU).

References

[1] H.S. Gutowsky, C.H. Holm, Rate processes and nuclear magnetic resonance spectra. II. Hindered internal rotation of amides, J. Chem. Phys. 25 (1956) 1228–1234.
[2] M.J. Bennett Jr, F.A. Cotton, A. Davison, J.W. Faller, S.J. Lippard, S.M. Morehouse, Stereochemically nonrigid organometallic compounds. I. π-Cyclopentadienyliron Dicarbonyl σ-cyclopentadiene1, J. Am. Chem. Soc. 88 (1966) 4371–4376.
[3] I. Bányai, Dynamic NMR for coordination chemistry, New J. Chem. 42 (2018) 7569–7581.
[4] A. Ault, The Bullvalene story. The conception of Bullvalene, a molecule that has no permanent structure, J. Chem. Educ. 78 (2001) 924.
[5] L. Mariño Pérez, F.S. Ielasi, L.M. Bessa, D. Maurin, J. Kragelj, M. Blackledge, N. Salvi, G. Bouvignies, A. Palencia, M.R. Jensen, Visualizing protein breathing motions associated with aromatic ring flipping, Nature 602 (2022) 695–700.

[6] R. Nepravishta, B. Yu, J. Iwahara, Hydrogen-exchange kinetics studied through analysis of self-decoupling of nuclear magnetic resonance, J. Magn. Reson. 312 (2020), 106687.
[7] A. Sekhar, L.E. Kay, An NMR view of protein dynamics in health and disease, Annu. Rev. Biophys. 48 (2019) 297–319.
[8] A.M. Jagger, C.A. Waudby, J.A. Irving, J. Christodoulou, D.A. Lomas, High-resolution ex vivo NMR spectroscopy of human Z α1-antitrypsin, Nat. Commun. 11 (2020) 6371.
[9] A.D. Gossert, W. Jahnke, NMR in drug discovery: A practical guide to identification and validation of ligands interacting with biological macromolecules, Prog. Nucl. Magn. Reson. Spectrosc. 97 (2016) 82–125.
[10] A. Furukawa, T. Konuma, S. Yanaka, K. Sugase, Quantitative analysis of protein–ligand interactions by NMR, Prog. Nucl. Magn. Reson. Spectrosc. 96 (2016) 47–57.
[11] R.Z. Pavlović, R.F. Lalisse, A.L. Hansen, C.A. Waudby, Z. Lei, M. Güney, X. Wang, C.M. Hadad, J.D. Badjić, From selection to instruction and back: competing conformational selection and induced fit pathways in abiotic hosts, Angew. Chem. Int. Ed Engl. 60 (2021) 19942–19948.
[12] R.R. Ernst, Principles of Nuclear Magnetic Resonance in One and Two Dimensions (International Series of Monographs on Chemistry): 14, Illustrated edition, Oxford University Press, 1997.
[13] G. Kaplan, J. Fraenkel, NMR of Chemically Exchanging Systems, 1st ed., Academic Press, 1980.
[14] A.D. Bain, Chemical exchange in NMR, Prog. Nucl. Magn. Reson. Spectrosc. 43 (2003) 63–103.
[15] A.G. Palmer, C.D. Kroenke, J.Patrick Loria, [10]- Nuclear magnetic resonance methods for quantifying microsecond-to-millisecond motions in biological macromolecules, in: T.L. James, V. Dötsch, U. Schmitz (Eds.), Methods in Enzymology, Academic Press, 2001, pp. 204–238.
[16] J. Sandström, Dynamic NMR Spectroscopy, Academic Press, 1982.
[17] E.R. Johnston, Density matrix theory for calculating magnetization transfer and dynamic lineshape effects, Concepts Magn. Reson. 7 (1995) 219–242.
[18] E.L. Kovrigin, NMR line shapes and multi-state binding equilibria, J. Biomol. NMR. 53 (2012) 257–270.
[19] P. Vallurupalli, A. Sekhar, T. Yuwen, L.E. Kay, Probing conformational dynamics in biomolecules via chemical exchange saturation transfer: a primer, J. Biomol. NMR. 67 (2017) 243–271.
[20] A.C. Sauerwein, D.F. Hansen, Relaxation Dispersion NMR Spectroscopy, in: L. Berliner (Ed.), Protein NMR: Modern Techniques and Biomedical Applications, Springer US, Boston, MA, 2015, pp. 75–132.
[21] D.F. Hansen, J.J. Led, Implications of using approximate Bloch-McConnell equations in NMR analyses of chemically exchanging systems: application to the electron self-exchange of plastocyanin, J. Magn. Reson. 163 (2003) 215–227.
[22] N.L. Fawzi, J. Ying, R. Ghirlando, D.A. Torchia, G.M. Clore, Atomic-resolution dynamics on the surface of amyloid-β protofibrils probed by solution NMR, Nature 480 (2011) 268–272.
[23] Y. An, S.L. Sedinkin, V. Venditti, Solution NMR methods for structural and thermodynamic investigation of nanoparticle adsorption equilibria, Nanoscale Adv 4 (2022) 2583–2607.
[24] V. Tugarinov, A. Ceccon, G.M. Clore, NMR methods for exploring “dark” states in ligand binding and protein-protein interactions, Prog. Nucl. Magn. Reson. Spectrosc. 128 (2022) 1–24.
[25] E.J. De Genst, T. Guilliams, J. Wellens, E.M. O'Day, C.A. Waudby, S. Meehan, M. Dumoulin, S.-T.D. Hsu, N. Cremades, K.H.G. Verschueren, E. Pardon, L. Wyns, J. Steyaert, J. Christodoulou, C.M. Dobson, Structure and properties of a complex of α-Synuclein and a single-domain camelid antibody, J. Mol. Biol. 402 (2010) 326–343.
[26] V.S. Dimitrov, J.A. Ladd, Dynamic NMR: Field dependence of the coalescence temperature and temperature dependence ofT2 Relaxation times inN,N-dimethyltrichloroacetamide, Magn. Reson. Chem. 23 (1985) 529–532.
[27] A. Moure, G. Sanclimens, J. Bujons, I. Masip, A. Alvarez-Larena, E. Pérez-Payá, I. Alfonso, A. Messeguer, Chemical modulation of peptoids: synthesis and conformational studies on partially constrained derivatives, Chemistry 17 (2011) 7927–7939.
[28] I. Alfonso, M.I. Burguete, S.V. Luis, A hydrogen-bonding-modulated molecular rotor: environmental effect in the conformational stability of peptidomimetic macrocyclic cyclophanes, J. Org. Chem. 71 (2006) 2242–2250.
[29] M.P. Williamson, Using chemical shift perturbation to characterise ligand binding, Prog. Nucl. Magn. Reson. Spectrosc. 73 (2013) 1–16.
[30] C.A. Waudby, A. Ramos, L.D. Cabrita, J. Christodoulou, Two-dimensional NMR lineshape analysis, Sci. Rep. 6 (2016) 24826.
[31] C.A. Waudby, T. Frenkiel, J. Christodoulou, Cross-peaks in simple two-dimensional NMR experiments from chemical exchange of transverse magnetisation, Angew. Chem. Int. Ed Engl. 58 (2019) 8784–8788.
[32] C.A. Waudby, M. Ouvry, B. Davis, J. Christodoulou, Two-dimensional NMR lineshape analysis of single, multiple, zero and double quantum correlation experiments, J. Biomol. NMR. 74 (2020) 95–109.
[33] G. Bodenhausen, D.J. Ruben, Natural abundance nitrogen-15 NMR by enhanced heteronuclear spectroscopy, Chem. Phys. Lett. 69 (1980) 185–189.
[34] K. Pervushin, R. Riek, G. Wider, K. Wüthrich, Attenuated T2 relaxation by mutual cancellation of dipole-dipole coupling and chemical shift anisotropy indicates an avenue to NMR structures of very large biological macromolecules in solution, Proc. Natl. Acad. Sci. U. S. A. 94 (1997) 12366–12371.
[35] A. Bax, R.H. Griffey, B.L. Hawkins, Correlation of proton and nitrogen-15 chemical shifts by multiple quantum NMR, J. Magn. Reson. 55 (1983) 301–315.
[36] P. Schanda, E. Kupce, B. Brutscher, SOFAST-HMQC experiments for recording two-dimensional heteronuclear correlation spectra of proteins within a few seconds, J. Biomol. NMR. 33 (2005) 199–211.
[37] V. Tugarinov, P.M. Hwang, J.E. Ollerenshaw, L.E. Kay, Cross-correlated relaxation enhanced 1H[bond]13C NMR spectroscopy of methyl groups in very high molecular weight proteins and protein complexes, J. Am. Chem. Soc. 125 (2003) 10420–10428.
[38] O.A. Gansow, J. Killough, A.R. Burke, Rate processes and carbon-13 magnetic resonance spectra. Hindered internal rotation of N,N-dimethyltrichloroacetamide, J. Am. Chem. Soc. 93 (1971) 4297–4298.
[39] G. Binsch, Unified theory of exchange effects on nuclear magnetic resonance line shapes, J. Am. Chem. Soc. 91 (1969) 1304–1309.
[40] A.D. Bain, D.M. Rex, R.N. Smith, Fitting dynamic NMR lineshapes, Magn. Reson. Chem. 39 (2001) 122–126.
[41] A.L. Parrill, gNMR version 3 for Macintosh, J. Chem. Inf. Comput. Sci. 36 (1996), 153–153.
[42] S.S. Stadmiller, J.S. Aguilar, C.A. Waudby, G.J. Pielak, Rapid quantification of protein-ligand binding via 19F NMR lineshape analysis, Biophys. J. 118 (2020) 2537–2548.
[43] A.I. Greenwood, M.J. Rogals, S. De, K.P. Lu, E.L. Kovrigin, L.K. Nicholson, Complete determination of the Pin1 catalytic domain thermodynamic cycle by NMR lineshape analysis, J. Biomol. NMR. 51 (2011) 21–34.
[44] H.M. McConnell, Reaction rates by nuclear magnetic resonance, J. Chem. Phys. 28 (1958) 430–431.
[45] A.D. Bain, B. Berno, Liouvillians in NMR: the direct method revisited, Prog. Nucl. Magn. Reson. Spectrosc. 59 (2011) 223–244.
[46] T.D. Alger, H.S. Gutowsky, R.L. Vold, Internal rotation in liquid 1-fluoro-1,1,2,2-tetrachloroethane, J. Chem. Phys. 47 (1967) 3130–3138.
[47] V. Římal, H. Štěpánková, J. Štěpánek, Analysis of NMR spectra in case of temperature-dependent chemical exchange between two unequally populated sites, Concepts Magn. Reson. Part A Bridg. Educ. Res. 38A (2011) 117–127.
[48] V. Březina, L. Hanyková, N. Velychkivska, J.P. Hill, J. Labuta, NMR lineshape analysis using analytical solutions of multi-state chemical exchange with applications to kinetics of host-guest systems, Sci. Rep. 12 (2022) 17369.
[49] H.S. Gutowsky, A. Saika, Dissociation, Chemical exchange, and the proton magnetic resonance in some aqueous electrolytes, J. Chem. Phys. 21 (1953) 1688–1694.
[50] N. Karschin, S. Krenek, D. Heyer, C. Griesinger, Extension and improvement of the methanol-d4 NMR thermometer calibration, Magn. Reson. Chem. 60 (2022) 203–209.
[51] S.S. Stadmiller, J.S. Aguilar, S. Parnham, G.J. Pielak, Protein-peptide binding energetics under crowded conditions, J. Phys. Chem. B. 124 (2020) 9297–9309.
[52] S.H.S. Chan, T. Włodarski, J.O. Streit, A.M.E. Cassaignau, L.F. Woodburn, M. Ahn, G.J. Freiherr von Sass, C.A. Waudby, N. Budisa, L.D. Cabrita, J. Christodoulou, The ribosome stabilizes partially folded intermediates of a nascent multi-domain protein, Nat. Chem. 14 (2022) 1165–1173.
[53] J.F. Thole, C.A. Waudby, G.J. Pielak, Disordered proteins mitigate the temperature dependence of site-specific binding free energies, J. Biol. Chem. (2023), 102984.
[54] C. Feng, E.L. Kovrigin, C.B. Post, NmrLineGuru: standalone and user-friendly GUIs for Fast 1D NMR lineshape simulation and analysis of multi-state equilibrium binding models, Sci. Rep. 9 (2019) 1–14.
[55] J. Rohonczy, Total lineshape analysis of DNMR spectra by IBM personal computer, Kem. Kozl. (1992). https://scholar.google.ca/scholar?cluster=8566445785964532474&hl=en&as_sdt=0,5&sciodt=0,5.
[56] iNMR, (n.d.). www.inmr.net (accessed February 20, 2023).
[57] H.J. Reich, WinDNMR: dynamic nmr spectra for windows, J. Chem. Educ. 72 (1995) 1086.
[58] N. Bampos, A. Vidal-Ferran, Understanding NMR multiplet structure with WinDNMR, J. Chem. Educ. Preview Publication DetailsPUBLICATION DETAILS × Scholarly J. J. Chem. Educ. Am. Chem. Soc. Citation/Abstract Coverage 66 (2000) 130–133.
[59] D.S. Stephenson, G. Binsch, Improved algorithm for the computation of exchange-broadened NMR bandshapes, J. Magn. Reson. 30 (1978) 625–626.
[60] C.A. Waudby, J. Christodoulou, NMR lineshape analysis of intrinsically disordered protein interactions, Methods Mol. Biol. 2141 (2020) 477–504.
[61] C.D. Cukier, D. Hollingworth, S.R. Martin, G. Kelly, I. Díaz-Moreno, A. Ramos, Molecular basis of FIR-mediated c-myc transcriptional control, Nat. Struct. Mol. Biol. 17 (2010) 1058–1064.
[62] M. Helgstrand, T. Härd, P. Allard, Simulations of NMR pulse sequences during equilibrium and non-equilibrium chemical exchange, J. Biomol. NMR. 18 (2000) 49–63.
[63] A.G. Palmer, J. Cavanagh, P.E. Wright, M. Rance, Sensitivity improvement in proton-detected two-dimensional heteronuclear correlation NMR spectroscopy, J. Magn. Reson. 93 (1991) 151–170.
[64] K.V. Pervushin, G. Wider, R. Riek, K. Wüthrich, The 3D NOESY-[^{1}H,^{15}N,^{1}H]-ZQ-TROSY NMR experiment with diagonal peak suppression, Proceed. Nat. Acad. Sci. 96 (1999) 9607–9612.
[65] A. Favier, B. Brutscher, Recovering lost magnetization: polarization enhancement in biomolecular NMR, J. Biomol. NMR. 49 (2011) 9–15.
[66] B. Shapira, A. Lupulescu, Y. Shrot, L. Frydman, Line shape considerations in ultrafast 2D NMR, J. Magn. Reson. 166 (2004) 152–163.
[67] U.L. Günther, B. Schaffhausen, NMRKIN: Simulating line shapes from two-dimensional spectra of proteins upon ligand binding, J. Biomol. NMR. 22 (2002) 201–209.

[68] M.W. Maciejewski, A.D. Schuyler, M.R. Gryk, I.I. Moraru, P.R. Romero, E.L. Ulrich, H.R. Eghbalnia, M. Livny, F. Delaglio, J.C. Hoch, NMRbox: a resource for biomolecular NMR computation, Biophys. J. 112 (2017) 1529–1534.
[69] J.P. Wurm, S. Sung, A.C. Kneuttinger, E. Hupfeld, R. Sterner, M. Wilmanns, R. Sprangers, Molecular basis for the allosteric activation mechanism of the heterodimeric imidazole glycerol phosphate synthase complex, Nat. Commun. 12 (2021) 2748.
[70] Y. Toyama, R.W. Harkness, L.E. Kay, Dissecting the role of interprotomer cooperativity in the activation of oligomeric high-temperature requirement A2 protein, Proceed. Nat. Acad. Sci. 118 (2021), e2111257118, https://doi.org/10.1073/pnas.2111257118.
[71] R. Creutznacher, T. Maass, J. Dülfer, C. Feldmann, V. Hartmann, M.S. Lane, J. Knickmann, L.T. Westermann, L. Thiede, T.J. Smith, C. Uetrecht, A. Mallagaray, C.A. Waudby, S. Taube, T. Peters, Distinct dissociation rates of murine and human norovirus P-domain dimers suggest a role of dimer stability in virus-host interactions, Commun. Biol. 5 (2022) 1–13.
[72] F.Ben Bdira, C.A. Waudby, A.N. Volkov, S.P. Schröder, E. Ab, J.D.C. Codée, H. S. Overkleeft, J.M.F.G. Aerts, H. van Ingen, M. Ubbink, Dynamics of ligand binding to a rigid glycosidase, Angew. Chem. Int. Ed Engl. (2020), https://doi.org/10.1002/anie.202003236.
[73] T.P. Dao, Y. Yang, M.F. Presti, M.S. Cosgrove, J.B. Hopkins, W. Ma, S.N. Loh, C. A. Castañeda, Mechanistic insights into enhancement or inhibition of phase separation by different polyubiquitin chains, EMBO Rep. 23 (2022) e55056.
[74] S. Alphonse, I. Djemil, A. Piserchio, R. Ghose, Structural basis for the recognition of the bacterial tyrosine kinase Wzc by its cognate tyrosine phosphatase Wzb, Proc. Natl. Acad. Sci. U. S. A. 119 (2022), e2201800119.
[75] A.C. McShan, K. Natarajan, V.K. Kumirov, D. Flores-Solis, J. Jiang, M. Badstübner, J.S. Toor, C.R. Bagshaw, E.L. Kovrigin, D.H. Margulies, N.G. Sgourakis, Peptide exchange on MHC-I by TAPBPR is driven by a negative allostery release cycle, Nat. Chem. Biol. 14 (2018) 811–820.
[76] H.R. Kunsch, The Jackknife and the Bootstrap for General Stationary Observations, Ann. Stat. 17 (1989) 1217–1241.
[77] J. Jeener, B.H. Meier, P. Bachmann, R.R. Ernst, Investigation of exchange processes by two-dimensional NMR spectroscopy, J. Chem. Phys. 71 (1979) 4546–4553.
[78] Y. Matviychuk, E. von Harbou, D.J. Holland, An experimental validation of a Bayesian model for quantification in NMR spectroscopy, J. Magn. Reson. 285 (2017) 86–100.
[79] C.A. Waudby, J. Christodoulou, Analysis of conformational exchange processes using methyl-TROSY-based Hahn echo measurements of quadruple-quantum relaxation, Magn. Reson. 2 (2021) 777–793.
[80] C.A. Waudby, C. Burridge, J. Christodoulou, Optimal design of adaptively sampled NMR experiments for measurement of methyl group dynamics with application to a ribosome-nascent chain complex, J. Magn. Reson. 326 (2021), 106937.
[81] G. Karunanithy, T. Yuwen, L.E. Kay, D.F. Hansen, Towards autonomous analysis of chemical exchange saturation transfer experiments using deep neural networks, J. Biomol. NMR. 76 (2022) 75–86.